Abdominal Radiology
https://doi.org/10.1007/s00261-024-04494-3

PELVIS

# Combining multimodal diffusion-weighted imaging and morphological parameters for detecting lymph node metastasis in cervical cancer

**Suixing Zhong[1] · Conghui Ai[1] · Yingying Ding[1] · Jing Tan[1] · Yan Jin[1] · Hongbo Wang[1] · Huimei Zhang[1] · Miaomiao Li[1] · Rong Zhu[1] · Shangwei Gu[1] · Ya Zhang[1]**

Received: 15 May 2024 / Revised: 5 July 2024 / Accepted: 6 July 2024


## Abstract

**Background** Accurate detection of lymph node metastasis (LNM) is crucial for determining the tumor stage, selecting optimal treatment, and estimating the prognosis for cervical cancer. This study aimed to assess the diagnostic efficacy of multimodal diffusion-weighted imaging (DWI) and morphological parameters alone or in combination, for detecting LNM in cervical cancer.

**Methods** In this prospective study, we enrolled consecutive cervical cancer patients who received multimodal DWI (conventional DWI, intravoxel incoherent motion DWI, and diffusion kurtosis imaging) before treatment from June 2022 to June 2023. The largest lymph node (LN) observed on each side on imaging was matched with that detected on pathology to improve the accuracy of LN matching. Comparison of the diffusion and morphological parameters of LNs and the primary tumor between the positive and negative LN groups. A combined diagnostic model was constructed using multivariate logistic regression, and the diagnostic performance was evaluated using receiver operating characteristic curves.

**Results** A total of 93 cervical cancer patients were enrolled: 35 with LNM (48 positive LNs were collected), and 58 without LNM (116 negative LNs were collected). The area under the curve (AUC) values for the apparent diffusion coefficient, diffusion coefficient, mean diffusivity, mean kurtosis, long-axis diameter, short-axis diameter of LNs, and the largest primary tumor diameter were 0.716, 0.720, 0.716, 0.723, 0.726, 0.798, and 0.744, respectively. Independent risk factors included the diffusion coefficient, mean kurtosis, short-axis diameter of LNs, and the largest primary tumor diameter. The AUC value of the combined model based on the independent risk factors was 0.920, superior to the AUC values of all the parameters mentioned above.

**Conclusion** Combining multimodal DWI and morphological parameters improved the diagnostic efficacy for detecting cervical cancer LNM than using either alone.

✉ Ya Zhang
sinvye@163.com

Suixing Zhong
1622146717@qq.com

Conghui Ai
656781921@qq.com

Yingying Ding
dingyingying0428@163.com

Jing Tan
2323338133@qq.com

Yan Jin
10285733@qq.com

Hongbo Wang
whb1024@sina.com

Huimei Zhang
1053209163@qq.com

Miaomiao Li
drlmm000@163.com

Rong Zhu
3142188134@qq.com

Shangwei Gu
1396097265@qq.com

[1] Department of Radiology, Yunnan Cancer Hospital, Third Affiliated Hospital of Kunming Medical University, No. 519, Kunzhou Road, Xishan District, Kunming 650118, China

Published online: 11 July 2024

**Graphical abstract**

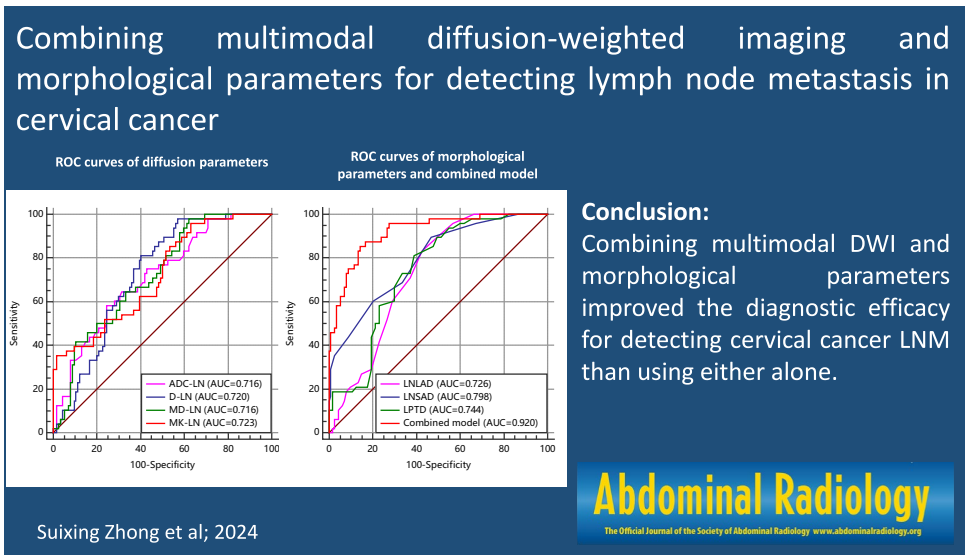


**Keywords** Uterine cervical neoplasms · Lymphatic metastasis · Diffusion magnetic resonance imaging

## Introduction

Cervical cancer is a common malignancy in women worldwide [1]. Despite widespread screening programs and well-established treatment options, the long-term survival rate of cervical cancer patients has not significantly improved due to lymph node metastasis (LNM) and other risk factors [2, 3]. According to the 2018 International Federation of Gynecology and Obstetrics (FIGO) staging system, radical hysterectomy with pelvic lymphadenectomy is one of the main treatments for early cervical cancer (FIGO stage IA-IB2 and IIA1) [4, 5]. However, the incidence of LNM in early cervical cancer is less than 20% [6, 7], and pelvic lymphadenectomy inevitably leads to lymphatic damage and postoperative complications, such as lymphoceles, infection, lower limb and perineal edema, neurovascular injury, and postoperative adhesion [8, 9]. This suggests that pelvic lymphadenectomy is unnecessary for the majority of early-stage cervical cancer patients. Furthermore, one of the most significant changes in the FIGO 2018 staging system is that cervical cancer patients with pelvic and/or para-aortic LNM are defined as at least stage IIIC and are no longer recommended for surgery but should undergo concurrent chemoradiotherapy [4, 5]. Therefore, pretreatment detection of LNM is crucial for clinical decision-making in cervical cancer patients.

Currently, sentinel lymph node biopsy is helpful for accurately assessing LNM, but its widespread clinical application is hindered by complex procedures [10]. Computed tomography (CT) and magnetic resonance imaging (MRI) are used to detect LNM in cervical cancer patients based on the criterion of an LN short axis ≥ 10 mm, which has a low sensitivity (62.2%) [11–13]. Positron emission tomography (PET) is more accurate in diagnosing LNM than CT and MRI, but it is expensive [14, 15].

Diffusion-weighted imaging (DWI) is a noninvasive imaging technique used to characterize tumors by exploiting the restricted diffusion of water molecules within proliferating tumor cells [16]. In recent years, advancements in magnetic resonance technology and mathematical algorithms have propelled the development of intravoxel incoherent motion DWI (IVIM-DWI) and diffusion kurtosis imaging (DKI) [17–19]. IVIM-DWI allows for the simultaneous assessment of water molecule diffusion and microcirculation perfusion in living tissues [17, 18], while DKI enables the quantification of non-Gaussian characteristics of water diffusion, providing a more accurate reflection of water molecule motion and distribution in biological tissues [19]. A few studies have indicated the potential value of IVIM-DWI and DKI in detecting LNM in cervical cancer patients [20–23]. However, these studies failed to accurately match LNs in terms of imaging and pathology, reducing the reliability of the results.

This study aimed to more accurately evaluate the diagnostic performance of multimodal DWI (DWI, IVIM-DWI, and DKI), morphological parameters, and their combination in detecting cervical cancer LNM by matching the

largest LN observed on each side by imaging with that observed via pathology.

## Methods

### Patients

This prospective study was approved by the local hospital ethics committee, and written informed consent was provided by each patient. A total of 93 patients were enrolled from June 1, 2022, to June 1, 2023. The inclusion criteria were as follows: (1) histopathologically confirmed cervical cancer; (2) MRI performed within 1 week before surgery, including routine sequences, IVIM-DWI, and DKI; (3) no other therapy administered before surgery; and (4) radical hysterectomy with pelvic lymphadenectomy after diagnosis. The exclusion criteria included (1) poor image quality and (2) neuroendocrine carcinoma and other rare pathological types.

### Imaging and data acquisition

MR imaging was performed using a Philips 3.0 T scanner (Ingenia, 3.0 T; Philips Medical Systems). A 10 mg aliquot of anisodamine was injected intramuscularly to reduce bowel peristalsis 5–10 min before the examination. All patients were scanned with an 8-channel, phased-array body coil in the supine position. The scanning sequence included T1-weighted imaging (T1WI) (axial plane), T2WI (axial, sagittal and coronal planes), DWI (axial plane, b-value = 800 s/mm$^2$), IVIM-DWI (oblique coronal plane), DKI (oblique coronal plane) and contrast-enhanced T1WI (axial, sagittal and coronal planes). The IVIM-DWI and DKI parameters were as follows.

IVIM-DWI was performed with a free-breathing single-shot spin-echo echo-planar sequence using 3-directional motion-probing gradients in the oblique coronal plane, and the scanning baseline was parallel to the long axis of the common iliac artery or sacrum. Repetition time/echo time: 9407 ms/60 ms; slice thickness/gap: 4 mm/1 mm; matrix: 128 × 128; field of view: 380 × 380 mm; number of slices: 24; number of excitations: 1; 11 b-values: 0, 20, 50, 100, 150, 500, 800, 1000, 1500 and 2000s/mm$^2$; and scan time: 12 min 14 s.

DKI was performed with a free-breathing single-shot spin-echo echo-planar sequence using 15-directional motion-probing gradients in the oblique coronal plane, and the scanning baseline was parallel to the long axis of the common iliac artery or sacrum. Repetition time/echo time: 2626 ms/100 ms; slice thickness/gap: 4 mm/1 mm; matrix: 128 × 128; field of view: 380 × 380 mm; number of slices: 24; number of excitations: 2; 3 b-values: 0, 800 and 1500 s/mm$^2$; and scan time: 6 min 33 s [24]. Saturation suppression technology was used when performing the IVIM-DWI and DKI scans to avoid motion artifacts.

### Imaging data analysis and processing

MR images were analyzed and measured independently by two radiologists with more than 5 years of experience in the imaging diagnosis of gynecological tumors. The largest primary tumor diameter (LPTD) and the LN long-axis diameter (LNLAD) were the widest diameters on any plane, and the LN short-axis diameter (LNSAD) was the maximum diameter perpendicular to the LNLAD.

The IVIM-DWI parameters were determined using the formula $Sb/S0 = (1 - f)\cdot\exp(-b\cdot D) + f\cdot\exp[-b\cdot(D + D^*)]$ [17], while the DKI parameters were calculated using the formula $S(b) = S0\bullet\exp(-b\bullet D + b^2\bullet D^2\bullet K/6)$ [19]. The DWI, IVIM-DWI, and DKI images were analyzed by using IMAgenGINE MRToolbox software (Vusion Tech Ltd.) [25]. With reference to the axial T2WI and contrast-enhanced images, the region of interest (ROI) was delineated on the DWI image with a b-value = 800 s/mm$^2$. All ROIs of the primary tumor and LN were delineated in the largest cross-sectional area of the lesion while avoiding all cystic and necrotic areas. The ROIs were automatically copied to the IVIM-DKI and DKI pseudocolored maps to obtain the apparent diffusion coefficient (ADC), diffusion coefficient (D), pseudodiffusion coefficient (D*), flowing blood volume fraction (f), mean diffusivity (MD), and mean kurtosis (MK) in each ROI. The mean parameter value for each ROI was used for analysis. The volumes and voxel counts of the LN ROIs ranged from 124.13–2587.67 μL to 26–542, respectively; the volumes and voxel counts of the primary tumor ROIs ranged from 238.71–10,196.30 μL to 50–2550, respectively.

### Surgical procedures and histopathological analysis

Radical hysterectomy combined with bilateral pelvic lymphadenectomy was performed by gynecological oncologists with more than 5 years of experience, and bilateral pelvic lymphadenectomy was performed from the deep circumflex iliac artery to the bifurcation of the abdominal aorta. All LNs were removed from 5 anatomical regions, including the external, internal, and common iliac vessels; the obturator; and the abdominal aorta. These LNs were divided into three groups: the left pelvic group, the right pelvic group, and the abdominal aorta group. The primary tumor and lymphadenectomy specimens were forwarded to the pathology department for standard histopathological analyses.

Following fixation in formalin and embedding in paraffin, the excised LNs were sliced into 5-μm-thick sections. These sections were subsequently stained with hematoxylin–eosin and assessed by two pathologists who had over 5 years of

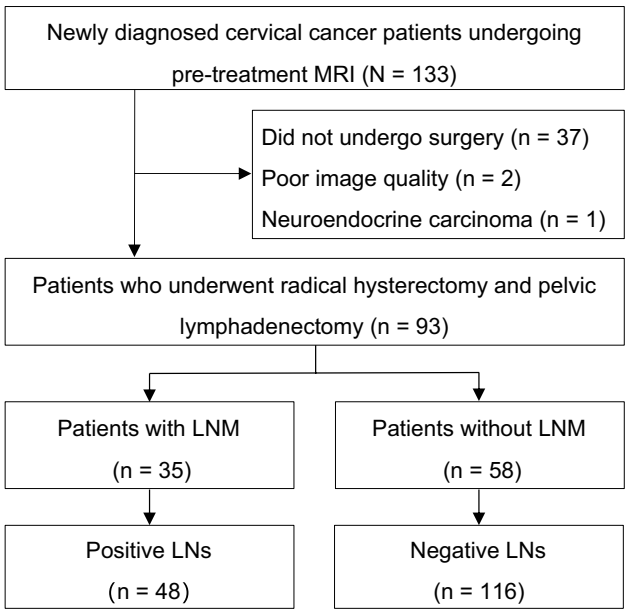


**Fig. 1** Study flowchart. *LNs* Lymph nodes, *LNM* lymph node metastasis, *MRI* magnetic resonance imaging

**Table 1** Patient clinical and pathological characteristics

| Characteristics | n = 93 |
|---|---|
| Median age (IQR), years | 48 (41–56) |
| Median number of dissected LNs (IQR) | 34 (28–41) |
| Pathological type | |
| Squamous cell carcinoma | n = 70 |
| Adenocarcinoma | n = 20 |
| Adenosquamous carcinoma | n = 3 |
| Patients with LNM | n = 35 |
| Patients without LNM | n = 58 |
| Positive LNs | n = 48 |
| Negative LNs | n = 116 |
| FIGO staging | |
| IA2 | n = 1 |
| IB1 | n = 14 |
| IB2 | n = 20 |
| IB3 | n = 10 |
| IIA1 | n = 8 |
| IIA2 | n = 5 |
| IIIC1p | n = 26 |
| IIIC2p | n = 9 |

*FIGO staging* international federation of gynecology and obstetrics (FIGO) staging, *IQR* interquartile range, *LN* lymph node, *LNM* LN metastasis

experience. A consensus was reached by discussion in the case of differences in opinion. The histopathological findings served as the diagnostic reference standard for this study.

**Table 2** Interobserver agreement between the two radiologists for morphological and diffusion parameters

| Parameters | ICC | 95% CI |
|---|---|---|
| LNLAD | 0.934 | 0.899–0.956 |
| LNSAD | 0.924 | 0.897–0.943 |
| ADC-LN | 0.891 | 0.821–0.930 |
| f-LN | 0.870 | 0.745–0.925 |
| D-LN | 0.843 | 0.790–0.883 |
| D*-LN | 0.915 | 0.758–0.959 |
| MD-LN | 0.889 | 0.821–0.928 |
| MK-LN | 0.883 | 0.741–0.937 |
| LPTD | 0.985 | 0.821–0.995 |
| ADC-tumor | 0.885 | 0.690–0.944 |
| f-tumor | 0.854 | 0.687–0.920 |
| D-tumor | 0.866 | 0.724–0.925 |
| D*-tumor | 0.862 | 0.783–0.909 |
| MD-tumor | 0.886 | 0.565–0.953 |
| MK-tumor | 0.867 | 0.707–0.928 |

*ADC-LN* apparent diffusion coefficient of lymph node, *ADC-tumor* apparent diffusion coefficient of tumor, *CI* confidence interval, *D-LN* diffusion coefficient of lymph node, *D-tumor* diffusion coefficient of tumor, *D*-LN* pseudodiffusion coefficient, *D*-tumor* pseudodiffusion coefficient of tumor, *f-LN* flowing blood volume fraction of lymph node, *f-tumor* flowing blood volume fraction of tumor, *ICC* interclass correlation coefficient, *LNLAD* lymph node long-axis diameter, *LNSAD* lymph node short-axis diameter, *LPTD* largest primary tumor diameter, *MD-LN* mean diffusivity of lymph node, *MD-tumor* mean diffusivity of tumor, *MK-LN* mean kurtosis of lymph node, *MK-tumor* mean kurtosis of tumor

## Correspondence between imaging and histopathology

On imaging, we measured only the largest LN in each pelvic LN group. Pathologically, we isolated and labeled the largest LN from each pelvic LN group and then the pathologists evaluated it. This ensures correspondence between the LNs detected by imaging and histopathology.

## Statistical analysis

All the data were analyzed by SPSS version 26.0 (SPSS Inc., Chicago, IL) and MedCalc version 20.0.22 (MedCalc Software bvba, Ostend, Belgium). As less than 5% of the data were missing, the handling of missing data was not applied. The interobserver agreement of the measurements between the two radiologists was assessed using the interclass correlation coefficient (ICC). An ICC > 0.80 was considered to indicate excellent agreement, and any parameter with an ICC below this threshold was excluded from further statistical analyses [26]. The mean value obtained from the measurements of both radiologists was utilized for further analysis.

**Table 3** Comparison of the morphological and diffusion parameters of positive and negative LNs

| Parameters | Positive LNs | Negative LNs | Statistic *z* | *P* value |
|---|---|---|---|---|
| LNLAD | 1.50 (1.20, 1.80) | 1.10 (0.80, 1.50) | −4.384 | < 0.001* |
| LNSAD | 0.80 (0.60, 1.10) | 0.50 (0.70, 0.40) | −5.926 | < 0.001* |
| ADC-LN | 0.75 (0.68, 0.85) | 0.87 (0.76, 1.04) | −4.333 | < 0.001* |
| f-LN | 0.20 (0.16, 0.25) | 0.21 (0.17, 0.26) | −1.201 | 0.230 |
| D-LN | 0.69 (0.65, 0.74) | 0.77 (0.69, 0.87) | −4.427 | < 0.001* |
| D*-LN | 24.13 (19.42, 32.06) | 20.57 (14.60, 29.45) | −1.329 | 0.184 |
| MD-LN | 1.06 (0.96, 1.20) | 1.22 (1.07–1.46) | −4.341 | < 0.001* |
| MK-LN | 0.98 (0.90, 1.35) | 0.90 (0.81, 1.00) | −4.110 | < 0.001* |
| LPTD | 3.80 (3.20, 4.40) | 2.95 (1.58, 3.60) | −4.789 | < 0.001* |
| ADC-tumor | 0.81 (0.76, 0.92) | 0.80 (0.70, 0.90) | −1.218 | 0.223 |
| f-tumor | 0.15 (0.13, 0.20) | 0.15 (0.13, 0.17) | −0.474 | 0.635 |
| D-tumor | 0.66 (0.64, 0.74) | 0.69 (0.62, 0.76) | −0.386 | 0.700 |
| D*-tumor | 27.69 (20.84, 37.57) | 27.11 (21.52, 34.51) | −0.458 | 0.647 |
| MD-tumor | 1.07 (0.93, 1.23) | 1.03 (0.94, 1.14) | −0.828 | 0.408 |
| MK-tumor | 0.94 (0.82, 1.01) | 0.87 (0.78, 1.01) | −1.222 | 0.222 |

*ADC-LN* apparent diffusion coefficient of lymph node, *ADC-tumor* apparent diffusion coefficient of tumor, *CI* confidence interval, *D-LN* diffusion coefficient of lymph node, *D-tumor* diffusion coefficient of tumor, *D*-LN* pseudodiffusion coefficient, *D*-tumor* pseudodiffusion coefficient of tumor, *f-LN* flowing blood volume fraction of lymph node, *f-tumor* flowing blood volume fraction of tumor, *ICC* interclass correlation coefficient, *LN* lymph node, *LNLAD* lymph node long-axis diameter, *LNSAD* lymph node short-axis diameter, *LPTD* largest primary tumor diameter, *MD-LN* mean diffusivity of lymph node, *MD-tumor* mean diffusivity of tumor, *MK-LN* mean kurtosis of lymph node, *MK-tumor* mean kurtosis of tumor

ADC, D, D*, and MD are in units of $10^{-3}$ $mm^2/s$. LNLAD, LNSAD, and LPTD are in units of cm. f and MK values have no units

The data are expressed as the median (interquartile range)

*$P < 0.05$

**Table 4** Analysis of independent risk factors for lymph node metastasis in cervical cancer patients

| Parameters | β | OR (95% CI) | *P* value |
|---|---|---|---|
| LNSAD | 0.476 | 1.609 (1.271–2.038) | < 0.001* |
| D-LN | −6.023 | 0.002 (0.000–0.419) | 0.022 |
| MK-LN | 4.304 | 74.028 (4.301–1274.047) | 0.003 |
| LPTD | 0.068 | 1.070 (1.031–1.112) | < 0.001* |

*β* standard regression coefficient, *CI* confidence interval, *D-LN* diffusion coefficient of lymph node, *LNSAD* lymph node short-axis diameter, *LPTD* largest primary tumor diameter, *MK-LN* mean kurtosis of lymph node, *OR* odds ratio

The analysis of all parameters was conducted at the LN level rather than at the patient level. Nonparametric Mann–Whitney *U* tests were used to compare all parameters between the positive and negative LN groups. Only statistically significant parameters in the univariate analysis were included in the receiver operating characteristic (ROC) curve analysis. Subsequently, the area under the curve (AUC), sensitivity, specificity, positive predictive value, negative predictive value, and accuracy were assessed. Variables with $P < 0.1$ from the univariate regression were entered into multivariate logistic regression analysis using forward stepwise regression based on maximum likelihood estimation. The DeLong test was used to compare the AUC values of different parameters. All the statistical analyses were conducted using a two-tailed test, and $P < 0.05$ indicated statistical significance.

## Results

A total of 93 cervical cancer patients were enrolled in the study. Pathology revealed that 35 patients had LNM (48 positive LNs were collected), and 58 patients had no LNM (116 negative LNs were collected) (Fig. 1). The patients' clinical and pathological characteristics are shown in Table 1. The two radiologists had excellent interobserver agreement, with ICCs ranging from 0.843 to 0.985 (Table 2).

Compared with the negative LN group, the positive LN group had greater LNLAD, LNSAD, MK of LN (MK-LN), and LPTD, but lower ADC of LN (ADC-LN), D of LN (D-LN), and MD of LN (MD-LN) (all $P < 0.001$). There were no statistically significant differences in the other parameters between the two groups (Table 3). The AUC values of LNLAD, LNSAD, MK-LN, LPTD, ADC-LN, D-LN, and MD-LN were 0.726, 0.798, 0.723, 0.744,

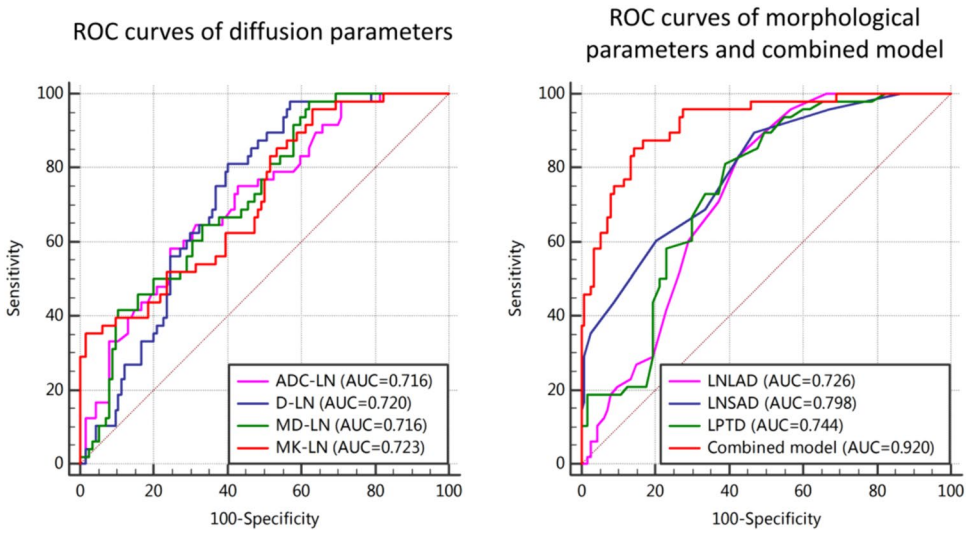


**Fig. 2** ROC curves of diffusion parameters, morphological parameters, and the combined model. There was no significant difference in the AUCs for the ADC-LN, D-LN, MD-LN, MK-LN, LNLAD, LNSAD, or LPTD. The AUC of the combined model, based on LNSAD, D-LN, MD-LN, and LPTD, surpassed that of the aforementioned six parameters. *ADC-LN* apparent diffusion coefficient of lymph node. *AUC* area under the curve, *D-LN* diffusion coefficient of lymph node, *LNLAD* lymph node long-axis diameter, *LNSAD* lymph node short-axis diameter, *LTPD* largest primary tumor diameter, *MD-LN* mean diffusivity of lymph node, *MK-LN* mean kurtosis of lymph node, *ROC* receiver operating characteristic

0.716, 0.720, and 0.716, respectively, with optimal cutoff values of 1.1 cm, 0.5 cm, 1.34, 3.1 cm, $0.76\times10^{-3}$ $mm^2/s$, $0.8\times10^{-3}$ $mm^2/s$, and $1.34\times10^{-3}$ $mm^2/s$, respectively (Table 4 and Fig. 2). The MR images of two cervical cancer patients with or without LNM in this study are shown in Fig. 3.

Multivariate logistic regression analysis indicated that the independent risk factors for LNM in cervical cancer patients were LNSAD, D-LN, MK-LN, and LPTD (Table 5). The AUC of the combined model based on these four independent risk factors was 0.920, with an optimal cutoff value of 0.31 (Table 4). The Delong test demonstrated no statistically significant differences in the AUCs of the LNLAD, LNSAD, MK-LN, LPTD, ADC-LN, D-LN, or MD-LN. The AUC of the combined model was superior to that of the aforementioned seven parameters ($P \leq 0.001$) (Fig. 2).

## Discussion

In this study, we accurately compared the diagnostic efficacy of multimodal DWI, morphological parameters, and their combination in detecting cervical cancer LNM by matching the largest LN observed on each side on imaging with that detected on pathology. The diagnostic performance of multimodal DWI parameters (ADC-LN, D-LN, MD-LN, and MK-LN) was comparable to that of morphological parameters (LNLAD, LNSAD, and LPTD). The independent risk factors for LNM in cervical cancer patients were LNSAD, D-LN, MK-LN, and LPTD. The diagnostic efficacy of the combined model based on these four risk factors was superior to that of multimodal DWI or morphological parameters alone.

In imaging studies involving LNM of cervical cancer, accurately matching LNs by imaging and histopathology is crucial. Xu et al. selected LNs with consistent numbers observed by both imaging and pathology [21]. Wu et al. correlated the largest LNs observed by imaging with the positive LNs identified via pathology [20]. Zhang et al. matched MR images with pathological results based on the size, shape, and location of LNs [23]. Yamada et al. matched LNs observed via MRI with those observed via pathology through visual and spatial comparisons of anatomical features [22]. However, a much greater number of LNs were detected by pathology than by imaging [27]. The largest LNs on imaging may not be positive LNs due to the presence of lymphadenitis and micrometastases [12, 28]. Therefore, the matching methods used in previous studies have a high possibility of misregistration. To minimize this, we measured only the largest LN observed on each side by imaging and isolated and labeled the largest LN via pathology, ensuring one-to-one correspondence between imaging and pathology.

Our study showed that positive LNs exhibited lower ADC-LN, D-LN, and MD-LN values and a greater MK-LN value than negative LNs. The diagnostic efficacy of these four parameters was comparable to that of morphological parameters (LNLAD, LNSAD, and LPTD). Xu et al.

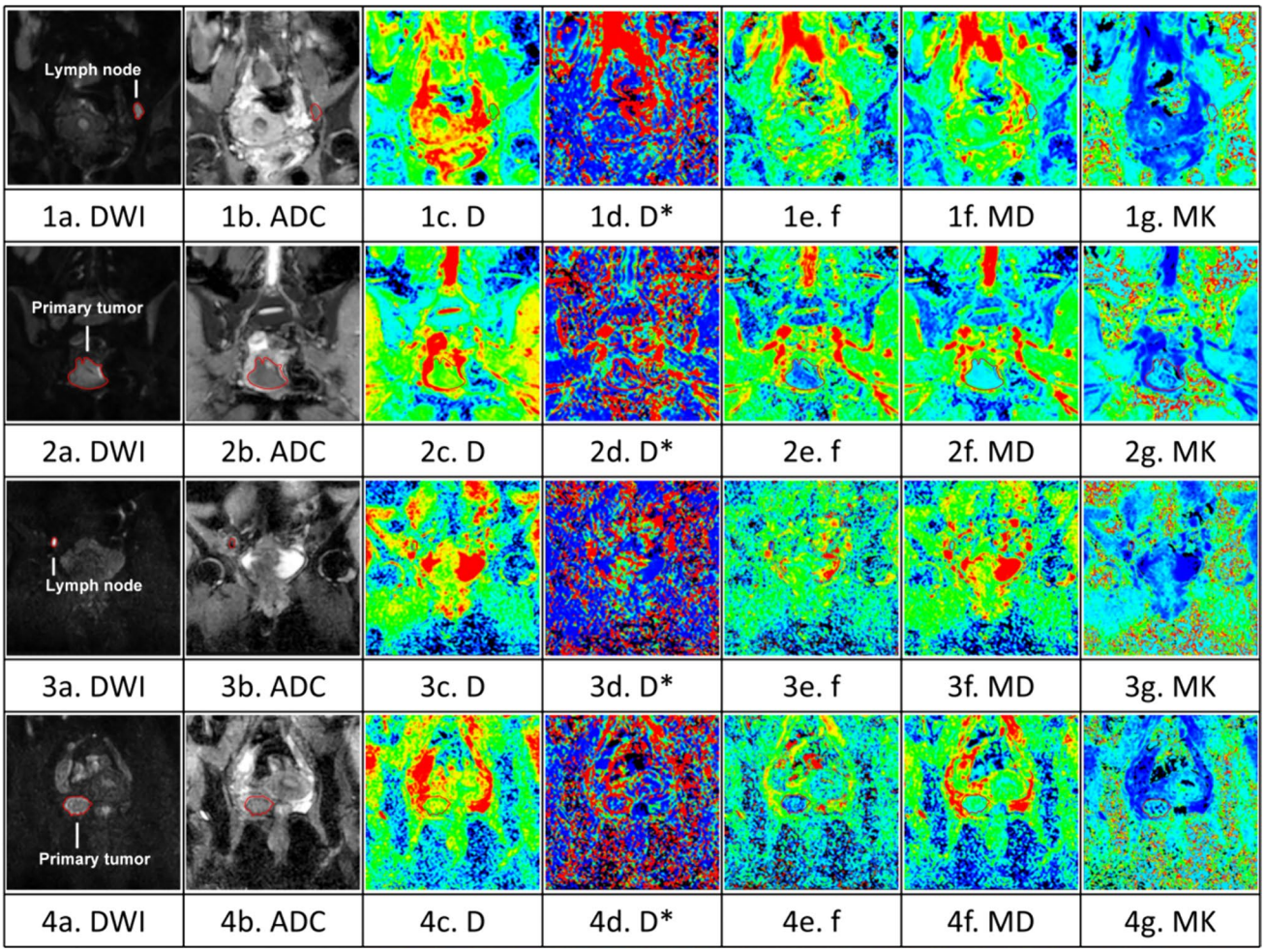


**Fig. 3** Multimodal diffusion-weighted imaging of two representative cases. **1a**–**1f** A 32-year-old female patient with cervical cancer and lymph node metastasis. Positive lymph node: LNLAD = 1.7 cm, LNSAD = 0.8 cm, ADC = $0.70 \times 10^{-3}$ $mm^2/s$, f = 0.14, D = $0.73 \times 10^{-3}$ $mm^2/s$, D* = $35.71 \times 10^{-3}$ $mm^2/s$, MD = $1.07 \times 10^{-3}$ $mm^2/s$, and MK = 0.85. Primary tumor: LPTD = 4.2 cm, ADC = $0.96 \times 10^{-3}$ $mm^2/s$, f = 0.14, D = $0.75 \times 10^{-3}$ $mm^2/s$, D* = $37.57 \times 10^{-3}$ $mm^2/s$, MD = $1.09 \times 10^{-3}$ $mm^2/s$, and MK = 0.82. **2a**–**2f** A 33-year-old female patient with cervical cancer without lymph node metastasis. Negative lymph node: LNLAD = 1.1 cm, LNSAD = 0.5 cm, ADC = $1.24 \times 10^{-3}$ $mm^2/s$, f = 0.17, D = $0.97 \times 10^{-3}$ $mm^2/s$, D* = $63.86 \times 10^{-3}$ $mm^2/s$, MD = $1.37 \times 10^{-3}$ $mm^2/s$, and MK = 0.54. Primary tumor: LPTD = 2.9 cm, ADC = $0.56 \times 10^{-3}$ $mm^2/s$, f = 0.12, D = $0.54 \times 10^{-3}$ $mm^2/s$, D* = $32.09 \times 10^{-3}$ $mm^2/s$, MD = $0.81 \times 10^{-3}$ $mm^2/s$, and MK = 1.00. *ADC* apparent diffusion coefficient, *D* diffusion coefficient, *D** pseudodiffusion coefficient, *f* flowing blood volume fraction, *LNLAD* lymph node long-axis diameter, *LNSAD* lymph node short-axis diameter, *LTPD* largest primary tumor diameter, *MD* mean diffusivity, *MK* mean kurtosis

indicated that the ADC-LN and D-LN were lower in positive LNs than in negative LNs [21]. Zhang et al. reported that positive LNs had lower ADC-LN than negative LNs [23]. Yamada et al. demonstrated that positive LNs exhibited lower ADC-LN and MD-LN and greater MK-LN than negative LNs [22]. Because ADC-LN, D-LN, and MD-LN represent the extent of water molecule diffusion within LNs, while MK-LNs represent the complexity of the LN structure [17–19], the consistent results above revealed that positive LNs have more restricted water molecule diffusion and more complex structures than negative LNs.

In our study, there was no difference in the f of LN (f-LN) or D* of LN (D*-LN) between positive and negative LNs. The f value is the flowing blood volume fraction, representing the proportion of capillaries in the tissue. D* is the pseudodiffusion coefficient, representing the diffusion rate of water molecules in microcirculation perfusion [17]. Xu and Wu et al. demonstrated that positive LNs had lower f-LN than negative LNs, and there was no difference in D*-LN between positive and negative LNs [20, 21]. Zhang et al. showed that positive LNs had higher f-LN and lower D*-LN than negative LNs [23]. Previous studies and our results revealed the instability of f-LN and D*-LN, which may be attributed to several reasons. The f value is closely related to the T2 time. This makes the f value relatively accurate in loose tissues (with a longer

**Table 5** Comparison of the diagnostic efficiency of morphological parameters, diffusion parameters, and the multivariable model

| Parameters | AUC (95% CI) | Optimal cutoff value | Sensitivity (%) | Specificity (%) | PPV (%) | NPV (%) | Accuracy (%) |
|---|---|---|---|---|---|---|---|
| LNLAD | 0.726 (0.650–0.801) | 1.2 | 83.3 | 56.9 | 44.4 | 89.2 | 64.6 |
| LNSAD | 0.798 (0.726–0.870) | 0.6 | 89.6 | 54.3 | 44.8 | 92.6 | 64.6 |
| ADC-LN | 0.716 (0.632–0.799) | 0.758 | 58.3 | 75.7 | 50.0 | 81.3 | 70.6 |
| D-LN | 0.720 (0.643–0.797) | 0.799 | 97.9 | 43.1 | 41.6 | 98.0 | 59.1 |
| MD-LN | 0.716 (0.635–0.796) | 1.344 | 97.9 | 37.9 | 39.5 | 97.8 | 55.5 |
| MK-LN | 0.723 (0.638–0.807) | 1.246 | 35.4 | 98.3 | 89.5 | 78.5 | 79.8 |
| LPTD | 0.744 (0.668–0.820) | 3.2 | 81.2 | 61.4 | 47.0 | 88.6 | 67.3 |
| Combined model | 0.920 (0.876–0.965) | 0.31 | 85.4 | 85.8 | 71.9 | 93.3 | 85.7 |

*ADC-LN* apparent diffusion coefficient of lymph node, *AUC* area under the curve, *CI* confidence interval, *D-LN* diffusion coefficient of lymph node, *LNLAD* lymph node long-axis diameter, *LNSAD* lymph node short-axis diameter, *LTPD* largest primary tumor diameter, *MD-LN* mean diffusivity of lymph node, *MK-LN* mean kurtosis of lymph node, *NPV* negative predictive value, *PPV* positive predictive value

Combined model: multivariable logistic regression model composed of LNSAD, D-LN, MD-LN, and LPTD

T2 time, such as the breast) but unstable in denser tissues (with a shorter T2 time, such as squamous cell carcinoma) [29–31]. Considering that the predominant histological type of cervical cancer in this study was squamous cell carcinoma, the f value may not be sufficiently stable. Additionally, due to the smaller volumes of LNs, especially those with fewer pixels, they are more susceptible to misregistration artifacts and partial volume effects from adjacent tissues [32].

The multivariate logistic regression analysis indicated that LNSAD, D-LN, MK-LN, and LPTD were independent risk factors for LNM in cervical cancer patients. A combined model based on these four parameters was constructed. To our knowledge, this is the first study to evaluate cervical cancer LNM by integrating IVIM-DWI, DKI, and morphological parameters. This combined model achieved superior diagnostic performance (AUC = 0.920) compared to either multimodal DWI or morphological parameters alone. Similarly, Xu et al. demonstrated that a combined model based on PET in LN diagnosis, total lesion glycolysis, and D-LN led to better diagnostic performance (AUC = 0.913) in detecting cervical cancer LNM than diffusion or PET parameters alone [33].

Although the combined model demonstrated favorable diagnostic performance, we still found some false positives (14.2%) and false negatives (14.6%). False positives might be caused by inflammatory LNs. These LNs showed enlargement due to inflammatory cell infiltration, reactive hyperplasia, and increased fibrous connective tissue, which restricted water molecule diffusion, resulting in similar diffusion and morphological parameters to positive LNs [34]. False negatives might be due to micrometastases. The presence of micrometastases meant that only a small portion of the ROI was replaced by tumor cells, while the remaining area remained normal. This less pronounced restriction of water molecule diffusion resulted in similar diffusion and morphological parameters to negative LNs.

The combined model has several advantages for clinical application. The major benefits are the rapid scan time of the IVIM-DWI and DKI sequences (less than 20 min) and the simplicity and convenience of their operation. This makes the model acceptable for patients and does not significantly increase the radiology department's workload. Additionally, its non-invasive nature enhances patient comfort, and not requiring contrast agents reduces the risk of allergic reactions. Furthermore, the MRI used in this model is radiation-free, allowing for repeated imaging without concerns about radiation exposure.

Our study has certain limitations. First, this study was conducted in a single center with a small sample size. Second, to ensure complete correspondence between imaging and pathology, we evaluated only the largest LN in each pelvic LN area; however, this approach may miss smaller positive LNs. Future studies should include more LNs while ensuring imaging-pathology matching to further improve diagnostic accuracy. Third, due to software limitations, we

could only depict the ROI of the lesion on two-dimensional images, not three-dimensional images, which may not represent the entire LN or tumor. Additionally, considering that over 80% of LNM in early-stage cervical cancer are smaller than 1 cm [35], a 4 mm slice thickness for multimodal DWI may be suboptimal in detecting some small LNM. Future studies should explore multimodal DWI sequences with thinner slice thicknesses and good image quality to improve the detection accuracy of smaller LNM. Lastly, the optimal scanning parameters for IVIM-DWI and DKI have not yet been determined. Further exploration and establishment of standard scanning parameters are needed to minimize the impact of scanning parameters on study results.

In conclusion, the diagnostic performance of multimodal DWI in detecting LNM in cervical cancer patients was comparable to that of morphological parameters. The diagnostic efficacy of combining multimodal DWI with morphological parameters was superior to that of multimodal DWI or morphological parameters alone.

**Funding** This study was funded by The scientific research fund project of Yunnan Education Department, 2021J0259, Ya Zhang, The Yunnan Provincial Science and Technology Department, 2019FE001-246, Jing Tan, 202001AY070001-071, Conghui Ai, 202101AY070001-184, Ya Zhang.

## References

1. Sung H, Ferlay J, Siegel RL, Laversanne M, Soerjomataram I, Jemal A, Bray F (2021) Global cancer statistics 2020: GLOBOCAN estimates of incidence and mortality worldwide for 36 cancers in 185 countries. CA-Cancer J Clin 71(3), 209–249. https://doi.org/10.3322/caac.21660
2. Kidd EA, Siegel BA, Dehdashti F, Rader JS, Mutch DG, Powell MA, Grigsby PW (2010) Lymph node staging by positron emission tomography in cervical cancer: relationship to prognosis. J Clin Oncol 28(12), 2108–2113. https://doi.org/10.1200/JCO.2009.25.4151
3. Twu NF, Ou YC, Liao CI, Chang WY, Yang LY, Tang YH, Chen TC, Chen CH, Chen TH, Yeh LS, Hsu ST, Chen YC, Chang CC, Cheng YM, Huang CY, Liu FS, Lin YS, Hsiao SM, Kan YY, Lai CH (2016) Prognostic factors and adjuvant therapy on survival in early-stage cervical adenocarcinoma/adenosquamous carcinoma after primary radical surgery: a Taiwanese gynecologic oncology group (TGOG) study. Surg Oncol 25(3), 229–235. https://doi.org/10.1016/j.suronc.2016.05.028
4. Bhatla N, Aoki D, Sharma DN, Sankaranarayanan R (2018) Cancer of the cervix uteri. Int J Gynecol Obstet 143(Suppl 2), 22–36. https://doi.org/10.1002/ijgo.12611
5. Bhatla N, Aoki D, Sharma DN, Sankaranarayanan R (2021) Cancer of the cervix uteri: 2021 update. Int J Gynecol Obstet 155(Suppl 1), 28–44. https://doi.org/10.1002/ijgo.13865
6. Bats AS, Buénerd A, Querleu D, Leblanc E, Daraï E, Morice P, Marret H, Gillaizeau F, Mathevet P, Lécuru F (2011) Diagnostic value of intraoperative examination of sentinel lymph node in early cervical cancer: a prospective, multicenter study. Gynecol oncol 123(2), 230–235. https://doi.org/10.1016/j.ygyno.2011.08.010
7. Salvo G, Ramirez PT, Levenback CF, Munsell MF, Euscher ED, Soliman PT, Frumovitz M (2017) Sensitivity and negative predictive value for sentinel lymph node biopsy in women with early-stage cervical cancer. Gynecol Oncol 145(1), 96–101. https://doi.org/10.1016/j.ygyno.2017.02.005
8. Querleu D, Leblanc E, Cartron G, Narducci F, Ferron G, Martel P (2006) Audit of preoperative and early complications of laparoscopic lymph node dissection in 1000 gynecologic cancer patients. Am J Obstet Gynecol 195(5), 1287–1292. https://doi.org/10.1016/j.ajog.2006.03.043
9. Achouri A, Huchon C, Bats AS, Bensaid C, Nos C, Lécuru F (2013) Complications of lymphadenectomy for gynecologic cancer. Ejso-Eur J Surg Onc 39(1), 81–86. https://doi.org/10.1016/j.ejso.2012.10.011
10. Bizzarri N, Obermair A, Hsu HC, Chacon E, Collins A, Tsibulak I, Mutombo A, Abu-Rustum NR, Balaya V, Buda A, Cibula D, Covens A, Fanfani F, Ferron G, Frumovitz M, Guani B, Kocian R, Kohler C, Leblanc E, Lecuru F, Leitao MM, Mathevet P, Mueller MD, Papadia A, Pareja R, Plante M, Querleu D, Scambia G, Tanner E, Zapardiel I, Garcia JR, Ramirez PT (2024) Consensus on surgical technique for sentinel lymph node dissection in cervical cancer. Int J Gynecol Cancer 34(4), 504–509. https://doi.org/10.1136/ijgc-2023-005151
11. Kim SH, Kim SC, Choi BI, Han MC (1994) Uterine cervical carcinoma: evaluation of pelvic lymph node metastasis with MR imaging. Radiology 190(3), 807–811. https://doi.org/10.1148/radiology.190.3.8115631
12. Paño B, Sebastià C, Ripoll E, Paredes P, Salvador R, Buñesch L, Nicolau C (2015) Pathways of lymphatic spread in gynecologic malignancies. Radiographics 35(3), 916–945. https://doi.org/10.1148/rg.2015140086
13. Salib MY, Russell JHB, Stewart VR, Sudderuddin SA, Barwick TD, Rockall AG, Bharwani N (2020) 2018 FIGO Staging classification for cervical cancer: added benefits of imaging. Radiographics 40(6), 1807–1822. https://doi.org/10.1148/rg.2020200013
14. Reinhardt MJ, Ehritt-Braun C, Vogelgesang D, Ihling C, Högerle S, Mix M, Moser E, Krause TM (2001) Metastatic lymph nodes in patients with cervical cancer: detection with MR imaging and FDG PET. Radiology 218(3), 776–782. https://doi.org/10.1148/radiology.218.3.r01mr19776
15. He T, Sun J, Wu J, Wang H, Liang C, Wang H, Li S, Su S (2022) PET-CT versus MRI in the diagnosis of lymph node metastasis of cervical cancer: a meta-analysis. Microsc Res Techniq 85(5), 1791–1798. https://doi.org/10.1002/jemt.24039
16. Song J, Hu Q, Huang J, Ma Z, Chen T (2019) Combining tumor size and diffusion-weighted imaging to diagnose normal-sized metastatic pelvic lymph nodes in cervical cancers. Acta Radiol 60(3), 388–395. https://doi.org/10.1177/0284185118780903
17. Le Bihan D, Breton E, Lallemand D, Aubin ML, Vignaud J, Laval-Jeantet M (1988) Separation of diffusion and perfusion in intravoxel incoherent motion MR imaging. Radiology 168(2), 497–505. https://doi.org/10.1148/radiology.168.2.3393671
18. Iima M, Le Bihan D (2016) Clinical intravoxel incoherent motion and diffusion MR imaging: past, present, and future. Radiology 278(1), 13–32. https://doi.org/10.1148/radiol.2015150244
19. Jensen JH, Helpern JA, Ramani A, Lu H, Kaczynski K (2005) Diffusional kurtosis imaging: the quantification of non-gaussian water diffusion by means of magnetic resonance imaging. Magnet Reson Med 53(6), 1432–1440. https://doi.org/10.1002/mrm.20508
20. Wu Q, Zheng D, Shi L, Liu M, Wang M, Shi D (2017) Differentiating metastatic from nonmetastatic lymph nodes in cervical cancer patients using monoexponential, biexponential, and stretched exponential diffusion-weighted MR imaging. Eur Radiol 27(12), 5272–5279. https://doi.org/10.1007/s00330-017-4873-1

21. Xu C, Du S, Zhang S, Wang B, Dong C, Sun H (2020) Value of integrated PET-IVIM MR in assessing metastases in hypermetabolic pelvic lymph nodes in cervical cancer: a multi-parameter study. Eur radiol 30(5), 2483–2492. https://doi.org/10.1007/s00330-019-06611-z
22. Yamada I, Oshima N, Wakana K, Miyasaka N, Wakabayashi A, Sakamoto J, Saida Y, Tateishi U, Kobayashi D (2021) Uterine cervical carcinoma: evaluation using non-Gaussian diffusion kurtosis imaging and its correlation with histopathological findings. J Comput Assist Tomo 45(1), 29–36. https://doi.org/10.1097/RCT.0000000000001042
23. Zhang Y, Zhang KY, Jia HD, Fang X, Lin TT, Wei C, Qian LT, Dong JN (2022) Feasibility of predicting pelvic lymph node metastasis based on IVIM-DWI and texture parameters of the primary lesion and lymph nodes in patients with cervical cancer. Acad Radiol 29(7), 1048–1057. https://doi.org/10.1016/j.acra.2021.08.026
24. Tang L, Zhou XJ (2019) Diffusion MRI of cancer: from low to high b-values. J Magn Reson Imaging 49(1), 23–40. https://doi.org/10.1002/jmri.26293
25 Yang M, Yan Y, Wang H (2019) IMAge/enGINE: a freely available software for rapid computation of high-dimensional quantification. Quant Imag Med Surg 9(2), 210–218. https://doi.org/10.21037/qims.2018.12.03
26. Landis JR, Koch GG (1977) The measurement of observer agreement for categorical data. Biometrics 33(1), 159–174. https://doi.org/10.2307/2529310
27. Liu Y, Liu H, Bai X, Ye Z, Sun H, Bai R, Wang D (2011) Differentiation of metastatic from non-metastatic lymph nodes in patients with uterine cervical cancer using diffusion-weighted imaging. Gynecol Oncol 122(1), 19–24. https://doi.org/10.1016/j.ygyno.2011.03.023
28. Lentz SE, Muderspach LI, Felix JC, Ye W, Groshen S, Amezcua CA (2004) Identification of micrometastases in histologically negative lymph nodes of early-stage cervical cancer patients. Obstet Gynecol 103(6), 1204–1210. https://doi.org/10.1097/01.AOG.0000125869.78251.5e
29. Liu C, Liang C, Liu Z, Zhang S, Huang B (2013) Intravoxel incoherent motion (IVIM) in evaluation of breast lesions: comparison with conventional DWI. Eur J Radiol 82(12), e782–e789. https://doi.org/10.1016/j.ejrad.2013.08.006
30. Zhang SX, Jia QJ, Zhang ZP, Liang CH, Chen WB, Qiu QH, Li H (2014) Intravoxel incoherent motion MRI: emerging applications for nasopharyngeal carcinoma at the primary site. Eur Radiol 24(8), 1998–2004. https://doi.org/10.1007/s00330-014-3203-0
31. Lemke A, Laun FB, Simon D, Stieltjes B, Schad LR (2010) An in vivo verification of the intravoxel incoherent motion effect in diffusion-weighted imaging of the abdomen. Magnet Reson Med 64(6), 1580–1585. https://doi.org/10.1002/mrm.22565
32. Yang X, Chen Y, Wen Z, Liu Y, Xiao X, Liang W, Yu S (2019) Non-invasive MR assessment of the microstructure and microcirculation in regional lymph nodes for rectal cancer: a study of intravoxel incoherent motion imaging. Cancer Imaging 19(1), 70. https://doi.org/10.1186/s40644-019-0255-z
33. Xu C, Li X, Shi Y, Wang B, Sun H (2020) Combinative evaluation of primary tumor and lymph nodes to predict pelvic lymphatic metastasis in cervical cancer: an integrated PET-IVIM MRI study. Cancer Imaging 20(1), 21. https://doi.org/10.1186/s40644-020-00298-y
34. Wang J, Liao Q, Zhang Y, Yu C, Bai R, Sun H (2012) Differential diagnosis of axillary inflammatory and metastatic lymph nodes in rabbit models by using diffusion-weighted imaging: compared with conventional magnetic resonance imaging. Korean J Radiol 13(4), 458–466. https://doi.org/10.3348/kjr.2012.13.4.458
35. Benedetti-Panici P, Maneschi F, Scambia G, Greggi S, Cutillo G, D'Andrea G, Rabitti C, Coronetta F, Capelli A, Mancuso S (1996) Lymphatic spread of cervical cancer: an anatomical and pathological study based on 225 radical hysterectomies with systematic pelvic and aortic lymphadenectomy. Gynecol Oncol 62(1), 19–24. https://doi.org/10.1006/gyno.1996.0184